Title

Application of full range swept source optical coherence tomography for imaging of the anterior eye segment in patients with type I Boston Keratoprosthesis

ISBN

9780819493408

Authors

Poddar, Raju
Cortes, Dennis
Zawadzki, Robert J
et al.

Publication Date

2013-03-20

DOI

10.1117/12.2006961

Peer reviewed

Application of Full Range Swept Source Optical Coherence Tomography for Imaging of the Anterior Eye Segment in Patients with Type I Boston Keratoprosthesis

Raju Poddar[1,2], Dennis Cortes[2], Robert J. Zawadzki*[1,2], Mark J. Mannis[2] and John S. Werner[1,2]
[1]Vision Science and Advanced Retinal Imaging Laboratory (VSRI) and
[2]Department of Ophthalmology & Vision Science, University of California Davis,
4860 Y Street, Ste. 2400, Sacramento, CA 95817, USA

ABSTRACTS

We present a high-speed complex conjugate resolved 1 μm swept source optical coherence tomography [SS-OCT] system using coherence revival of the light source for clinical imaging of the anterior segment of the eye. High-speed of 100,000 A-scans/sec and 1 μm imaging window of OCT permits dense 3D imaging of the anterior segment, minimizing the influence of motion artifacts and deep penetration of images for topographic analysis. The swept laser performance with internal clocking was adapted to achieve extended imaging depth requirements. The feasibility of our instrument for visualization of the anterior segment of patients with the Boston Keratoprosthesis (KPro) was discussed. The relations between of the KPro and the surrounding tissue were also demonstrated.

Keywords: optical coherence tomography; ophthalmology; imaging system; medical optics instrumentation; keratoprosthesis

1. INTRODUCTION

The CAS (cornea and anterior segment) imaging system first introduced for time domain OCT, (Carl Zeiss, Inc.) used a light source with a central wavelength of 830 nm, and was able to reconstruct cross-sectional images of only a small portion of the anterior segment, with an imaging speed of 100-400 lines/s [1]. Then in 2000 [2], an OCT system uses 1310 nm superluminescent diode capable of covering larger portion of the anterior segment entire cross-sectional information about the cornea was reported. A few years later a commercial 1310 nm time-domain OCT system for *in vivo* anterior segment imaging was launched, Visante OCT (Carl Zeiss, Inc.), with axial resolution of 18 μm and an imaging speed of 2000 lines/s. The introduction of Fourier-domain OCT [3-5], with the advantage of increased sensitivity and acquisition speed permitted three-dimensional imaging [6-9] with short depth range [~ 2 mm in tissue]. Nowadays, most of the commercial Fourier-domain OCT systems using a spectrometer (Spectral OCT–SOCT) have reached an axial resolution of 3-6 μm and imaging speeds of 20,000–50,000 lines/s, like SPECTRALIS (Heidelberg Engineering) with axial resolution of 3.9 μm and an imaging speed of 40,000 lines/s and scan depth 1.9 mm [10], SS-1000 "CASIA" (TOMEY Corp.) etc [11], but they are not able to provide adequate assessment of anterior and posterior corneal topography because of strong fringe washout and sensitivity drop off typical for SOCT [12-14].

Swept source OCT (SS-OCT), uses a wavelength tunable lasers to provide improved imaging speed and higher sensitivity in comparison with previous OCT technologies [15]. For SS-OCT two modalities, have been used for wavelength sweeping: diffraction grating with polygonal mirror [16-18] or fiber Fabry-Perot tunable filter [19, 20]. SS-OCT with Fourier domain mode locking (FDML) lasers achieved a repetition rate of up to several Megahertz [21-24]. The major advantage for 1μm 100 kHz SSOCT apart from improved speed and sensitivity is better tissue penetration for imaging of iris, sclera, or irido-scleral angle. Recently, Topcon introduced an instrument DRI OCT-1, based on SS-OCT with axial resolution of 9 μm and a scanning speed of 100,000 lines/s for posterior segment evaluation [25]. But, the application is limited to posterior segment and short depth range [~2mm].

Currently, there is demand in clinical and interventional ophthalmic practice for imaging, the full architecture of the cornea, iris and the crystalline lens. Large-scale imaging covering the depth of ~8 mm in tissue and a large (15 x 15mm) transverse range enables quantification of morphometric parameters including the corneal thickness and topography, corneo-scleral angle, orientation of intraocular lenses, etc. In clinical settings precise quantitative assessment of anterior segment is also critical, such as for the KPro lens implant.

*rjzawadzki@ucdavis.edu; phone 1 916 734-5839; fax 1 916 734-5839; http://vsri.ucdavis.edu/

Optical Coherence Tomography and Coherence Domain Optical Methods in Biomedicine XVII,
edited by James G. Fujimoto, Joseph A. Izatt, Valery V. Tuchin, Proc. of SPIE Vol. 8571, 85713C

Knowledge of the exact corneal shape is essential, not only to determine a patients' suitability to undergo surgery, but also to properly plan the treatment. Our goal is to develop a robust high-speed volumetric SS-OCT system that extends our ability to image and evaluate in 3D the full depth of the anterior segment of the human eye. This type of imaging has the potential to provide significant information either on particular anatomical details or full range architecture of the cornea, iris and the crystalline lens.

Keratoprosthesis (KPro) has been recognized as a viable alternative to penetrating keratoplasty in the treatment of selective patients with corneal blindness, particularly after repeated graft failures. The Boston KPros are illustrated in Figure 1. KPro [26-30] includes a protruding cylinder that passes through an opening in the eyelid. A donor cornea is placed between the front and back plates, and the combination is sutured into the patient's corneal opening. The holes in the back plate allow the aqueous humor to diffuse into the donor cornea.

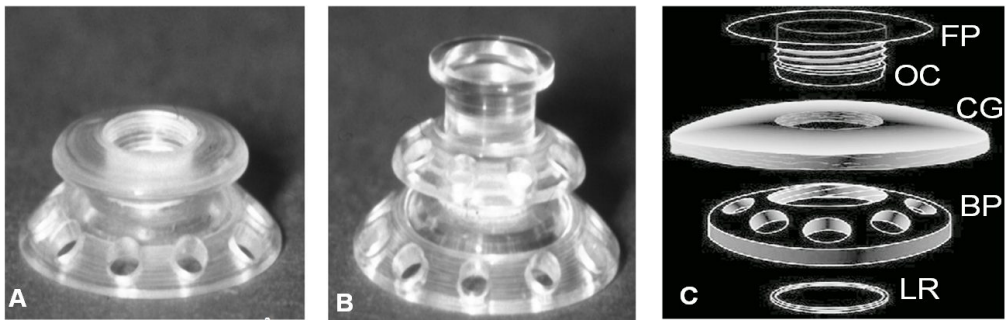

Fig. 1. Images of Boston Keratoprosthesis (KPro) Type 1 (A) and Type 2 (B). Different components of KPro (c), FP: Front Plate, OC: Optical Cylinder, CG: Corneal Graft, BP: Back Plate, HC: Peripheral Host Cornea and LR: Locking Ring.

During surgery, a donor corneal graft is used as a carrier with a 3-mm central hole, through which the optical cylinder of the KPro is inserted. The back plate of the KPro is either screwed onto the stem to produce firm apposition with the donor tissue, or snapped onto the stem with no rotating movement. A titanium locking ring is snapped in place behind the back plate to prevent loosening of the back plate. The graft-prosthesis combination is then transferred to the patient's trephined corneal opening and sutured in place. Finally, for the Type 1 KPro, a soft contact lens (usually a Kontur lens; Kontur Kontact Lens Co., Hercules, CA), 16 mm diameter and 9.8 mm base curve, plano power, is placed as a bandage lens. The Type 2 KPro (Fig. 1b) has an anterior cylinder, enabling it to protrude through an opening in the closed lid (Fig. 1c). Type 2 is rarely used, and then only in end-stage dry eye. Up to now only few reports on in-vivo imaging of KPro lens implantation and evaluations have been published with limited field of view.

Better understanding of visual function with the KPro may lead to design and practice modifications that will further improve surgical outcomes. This is why we decided to use our clinical anterior eye imaging complex conjugate free Swept Source OCT system for in-vivo evaluation of implantation of KPro lens.

2. MATERIALS AND METHODS

2.1. SSOCT system

A schematic diagram of our 1μm SSOCT system is shown in Figure 2. An external cavity tunable laser (ECTL), swept-source laser (Axsun Technologies), with a central wavelength of 1060nm, sweep bandwidth of 110 nm, repetition rate of 100 kHz, 46% duty cycle and average output power of ~23 mW, was used as the light source. A spectrally balanced interferometer configuration was used with three 50/50 fiber couplers (AC Photonics), and a balanced Michelson fiber interferometer was constructed [31]. The sample port was attached to a probe unit, which comprises a fiber collimator lens (12.38 mm, focal length, TC12APC-1064, Thorlabs, Inc.), two-axis galvano mirror (Cambridge Technology), and an achromatic doublet with a focal length of 75 mm (Thorlabs, Inc.). The reference port of the coupler is attached to a reference unit comprising a collimator lens, an achromatic doublet lens, dispersion compensating block and a static silver-coated mirror.

The galvanometric scanner steering the probe beam is controlled by a function generator board (PCI-6363, National Instruments, TX). The probing beam power at the sample was set as 1.85 mW, which is lower than the ANSI standard for safe exposure limit. The reflected beams from both arms are combined at the coupler and detected by a balanced photodetector with a bandwidth of DC to 1GHz (Wiserlabs, WL-BPD1GA) followed by RF amplifier (Minicircuits ZFL-1000+).

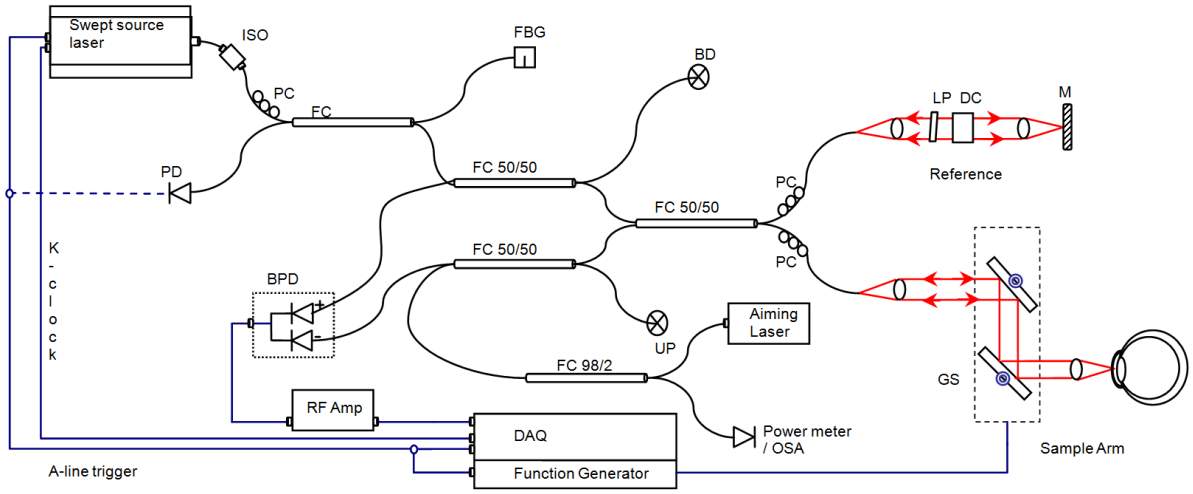

Fig. 2. Schematic of SSOCT system. Swept source laser 1060nm Axsun ECTL. FBG: Fabry Bragg Grating, FC: Fiber Coupler, GS: galvanometer scanning mirrors, DC: dispersion compensating materials, M: mirror, BPD: balanced receiver, PC: polarization controller, LP: polarizer, RF Amp: RF amplifier, BD: Beam dump, UP: unused port, OSA: optical spectrum analyzer, DAQ: digitizer.

2.2. Sample clocking, wavelength calibration and system performance

The interference signal is digitized by a data acquisition (DAQ) board with 8-bit resolution and a maximum sampling rate of 1 GS/s (ATS9870, AlazarTech, QC, Canada). Both the clock and receiver signals were digitized using custom designed LabVIEW software. The clock signal was then up-sampled and the maxima-minima and zero crossings of the first derivative were recorded. The receiver data were then resampled to be linear with respect to the intervals of these zero-crossings. It was found that the laser sweep was sufficiently stable that, for real time image display in LabVIEW, only the clock corresponding to the first A-scan for every B-scan needed to be processed, and signals for all other A-scans could be resampled according to the calibration from this first A-scan. However, every clock signal was recorded and stored for use in post-processing [32].The SS-OCT signal was sampled linearly in time, and the lasers swept nonlinearly in wavenumber, the acquired signal required resampling before Fourier transformation. The Axsun 1060 nm OCT engine contained an internal Mach-Zehnder interferometer clock, whose signal was digitized along with the photoreceiver signal. The maxima, minima and zero-crossings of the clock were detected and used to generate a linear-in-wavenumber recalibration vector that was used to resample the SSOCT signal linearly in wavenumber. However, because the clock signals were only intended for imaging depths of 3.7 mm (using 1376 sample points), the recalibration vector was first interpolated to increase the achievable imaging depth 12.4 mm using the k-clock signal [acquired 1GS/sec digitizer card, 4608 points]. For real time display the photoreceiver signals were then resampled using this recalibration vector via linear interpolation. After the recalibration there is axial PSF degradation, analogous to the effects of material dispersion. These dispersion-like effects, as well as true dispersion from unmatched optics and fiber lengths in the sample and reference arm, were corrected using numerical dispersion compensation. Briefly, after resampling to linearize the spectral interferogram in wavenumber, the spectral interferogram was multiplied by a complex phase function, given by:

$$I(k) = \exp(-j(a_1(k - k_0)^2 + a_2(k - k_0)^3)) \quad (1)$$

where, a_1 and a_2 are fitting parameters and k0 is the central wavenumber of the sweep. Optimal values of a_1 and a_2 were determined using an optimization algorithm to maximize the peak signal from a mirror.

Fall-off profiles from the 1060 nm system were tested. A peak sensitivity of 98 dB was measured near the 0 cavity offset with 1.8 mW incident on the sample. The theoretical shot noise limit for this system was also 104 dB, and the discrepancy between the measured and theoretical sensitivity was due to the same factors discussed above, as well amplification noise from the RF amplifier.

3. Results and Discussion Three dimensional imaging anterior segment of normal human eye

For purposes of this study, two healthy eyes and two eyes with Keratoprosthesis implants were imaged without pupil dilation. Written informed consent was obtained under protocols approved by the Institutional Review Board of the University of California Davis. The light power of light impinging on the eye was set to 1.85 mW, below the safety requirements of the ANSI standards. Several different scan protocols designed for imaging specific features in the anterior segment were used. In this paper we are presenting examples of two- and three- dimensional images and OCT movies in healthy eye and with KPro implants. In the cross-sectional images the intensity of light scattered and/or reflected from the internal structures within the sample was coded in a grey scale. Our three-dimensional data visualization software (IDAV 1.0) was used.

Using the high-resolution mode it is possible to visualize detailed morphology in different areas of the anterior segment. In Fig. 3 (A and B) an example of a high quality cross-sectional image of the junction between the cornea and sclera of is shown. For this purpose a configuration with a 30 mm focal length scan lens was placed after the galvo scanners. The short imaging range (3.4 mm in tissue) configuration that uses a digital storage scope sampling at 500 mega sample per second (MSPS) using external k-clock triggering with 1376 points. The final images were generated by averaging of 10 frames. The trabecular meshwork (TM) and Schlemm's canal (SC) itself can be seen in the full size. Deep image penetration enables visualization of the iris and anterior angle through the sclera. The 1060nm imaging system achieves considerably higher axial resolution of 5.6μm. The OCT image (B-scan) consists of 2,000 A-scans. Each tomogram line was acquired within 5 μs. Resolution of the system is sufficient to distinguish epithelium and delineate the position of the Bowman's membrane. The scanning protocol of 100 B-scans with 1000 A-scans each was chosen for this purpose.

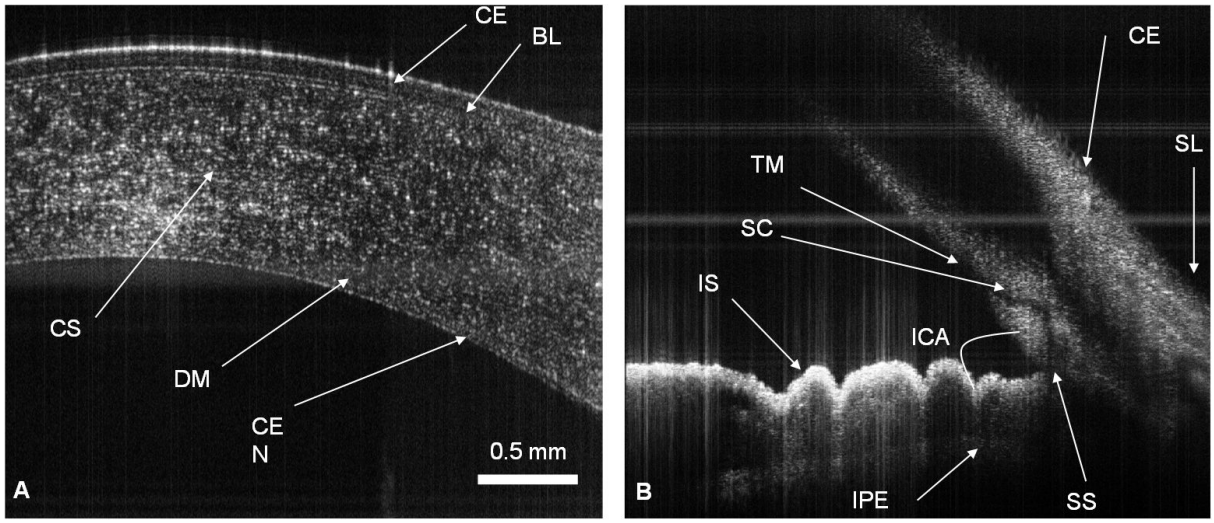

Fig. 3. Cross-sectional images of human anterior eye segments (A) Cornea [3.5mm x 1.5 mm]; CE: corneal epithelium, BL: Bowman's layer, CS: corneal stroma, DM: Descemet's membrane, CEN: Corneal endothelium (B) Irido-corneal angle [3.5 x 2.2mm]; SL: sclera, IS: iris stroma, IPE: iris pigment epithelium, SS: scleral spur, TM: trabecular meshwork, SC: Schlemm's canal, and ICA: iridocorneal angle opening.

Figure 4 (A) shows a cross sectional image from the full imaging range (11.5 mm in air) configuration that uses a digital storage scope sampling at 1 GSPS. The image consists of 4608 axial scans over 15mm and shows the cornea, iris, and anterior surface of the lens in a single image. The long imaging range is enabled by the long coherence length of the short cavity laser and high 1 GSPS rate of the oscilloscope acquisition. A longer focal length scan lens (75mm) was used to increase the Raleigh range (depth of focus) of this configuration to match the long imaging range; however, the larger resulting spot compromises lateral resolution. Figure 4 B-D visualized Volumetric Data set acquired with the same configuration. A fixed pattern noise visible on our images appears to originate from the swept laser source and results in multiple horizontal lines across the image. Background subtraction and post-processing help to reduce this noise, but doesn't eliminate it. The ability to image over a long range and with high axial and lateral resolution opened possibility to visualize the whole anterior eye with KPro implants.

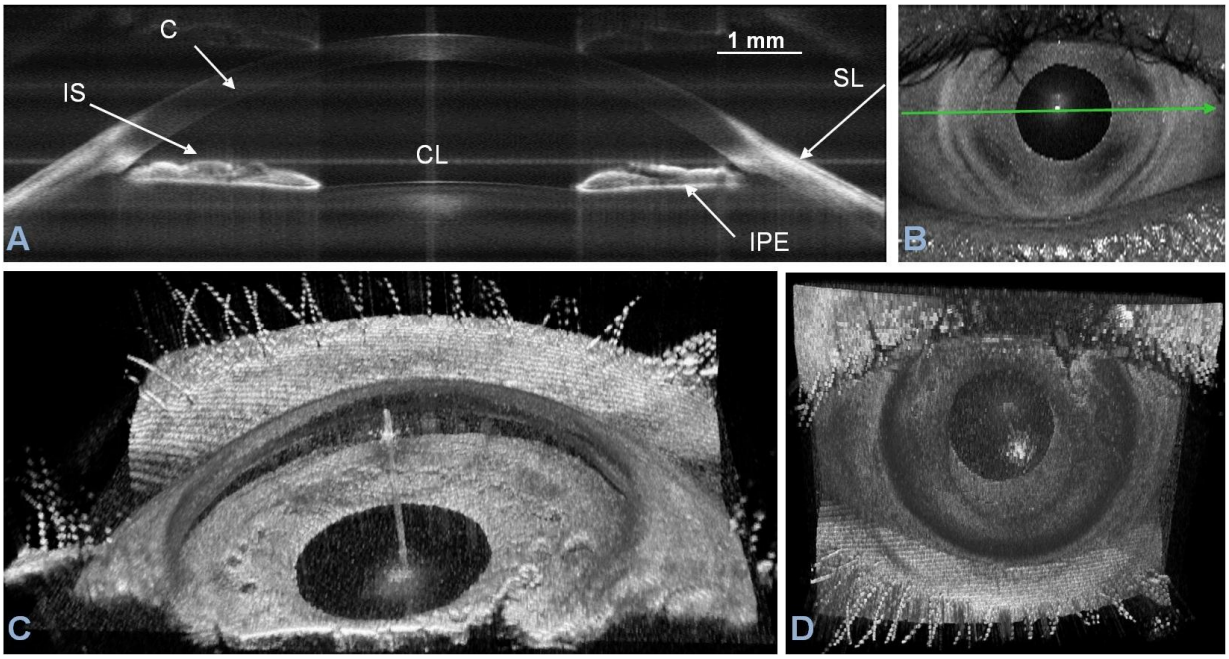

Fig. 4. Full imaging range mode: A. Cross-sectional image of the anterior chamber together with cornea and anterior surface of crystalline lens [image comprise 2000 x 2300 pixels spanning 14 mm (lateral) x 6.9 mm (axial). Each image represents 5 averaged frames. obtained over 100msec. C: Cornea, corneal epithelium, SL: sclera, IS: iris stroma, IPE: iris pigment epithelium, CL: crystalline lens]; Large-scale three-dimensional reconstruction of the anterior segment of human eye [B, C and D] in vivo: en face view (3-D rendering) [Images are reconstructed from 1000 × 100 × 2048 voxel data set. The size of the imaged volume is 15 × 20 × 7.5 mm.]

3.2. Three dimensional imaging anterior segment with KPro lens implantation

Existing technology for imaging of in-vivo anterior segment using the Spectralis™ AS-OCT is based on acquisition speed of 40,000 A-scans per second with an axial resolution of 3.9-7 μm and a transverse resolution of 14 μm. It has higher resolution and image acquisition time, compared with time-domain OCT systems such as the VisanteTM (Carl Zeiss AG, Germany), (lower axial resolution of 18 μm and a transverse resolution of 60 μm). The limitations associated with the Spectralis™ are a shallow scan depth (only 1.9 mm), image acquisition speed and poor ability to penetrate tissues that produce high light scatter (e.g., sclera, limbus). These limitations prevent the Spectralis™ AS-OCT from capturing a cross-section of the entire anterior segment (entire cornea or KPro) in one image. To overcome those limitations, here we develop an adjust able imaging range (2.5-8.5mm in tissue) with 7 μm axial resolution, higher image acquisition speed and deep tissue penetration. This new system can acquire the full anterior segment with KPro implantation.

3.2.1. Imaging with short focal length (30 mm) objective lens and external clocking:

Using this imaging mode (imaging depths of 2.6mm in tissue and1376 sample points), we obtained high-resolution images of the KPro, visible as a T-shaped cylinder with corrugated sides through the center of the cornea (Fig. 5). The bandage contact lens, front plate, optical cylinder, back plate, the carrier corneal graft and the graft host junction were distinctly visualized in the images obtained (Fig. 5). This high-resolution mode reveals epithelium behind the front plate (Fig. 5D). We can also see the endothelial layer (Figure 5E, red arrow). It has also the potential to detect the presence of retroprosthetic membrane, epithelial lip over the periphery of the anterior surface of the KPro front plate periprosthetic cysts, gaps or spaces of KPro eyes. In a single image we can observe the contact lens, KPro and iris, which were not possible at the slit lamp and Spectralis™. We can also study the corneal thinning in the carrier graft. The holes in the back plate were visible in all KPro eyes (Fig. 5E).

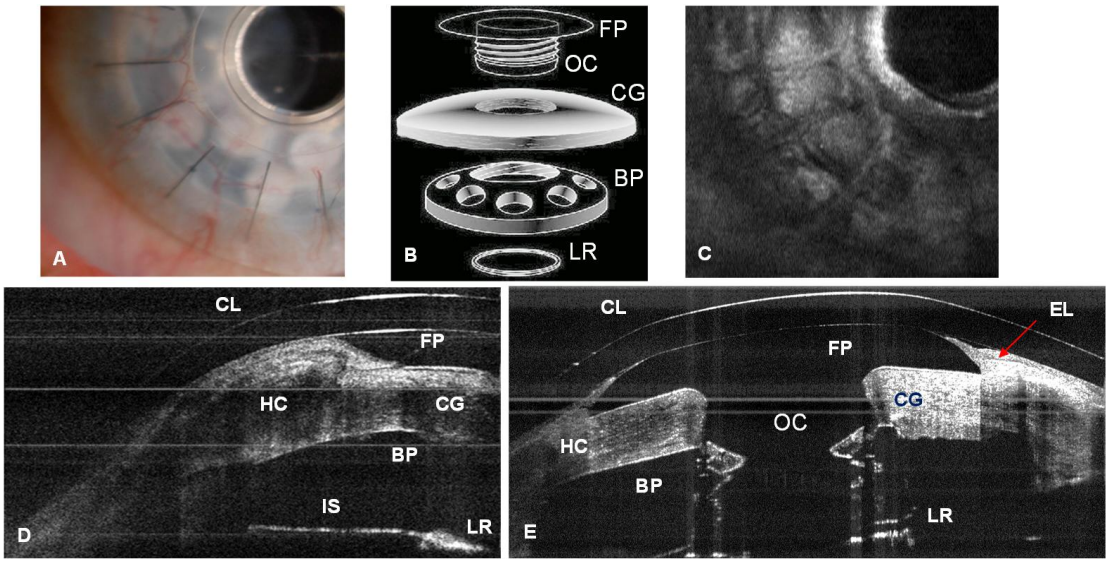

Fig. 5. In-vivo implantation of type I KPro lens (A), en face view (3-D rendering) of implants (B), en face view of the backplate of KPro lens (C); Cross-sectional images of Irido-corneal angle of KPro implants (D) [3.5mm x 2.5 mm comprises of 2000x1024 pixels]; Corneal portion [7.5mm x 2.5 mm comprises of 1000x1024 pixels]; Each image represents 5 averaged frames. FP: Front Plate, OC: Optical Cylinder, CG: Corneal Graft, BP: Back Plate, HC: Peripheral Host Cornea, LR: Locking Ring IS: Iris.

3.2.2. Imaging with long focal length (75mm) objective lens and internal clocking:

By using the extended depth range (k-clock signal acquired 1GS/sec digitizer card, 4608 points), we obtained full images of KPro implants (contact lens, front plate back plate, optical cylinder, locking ring and Iris) in a single B-scan (Fig. 6D).

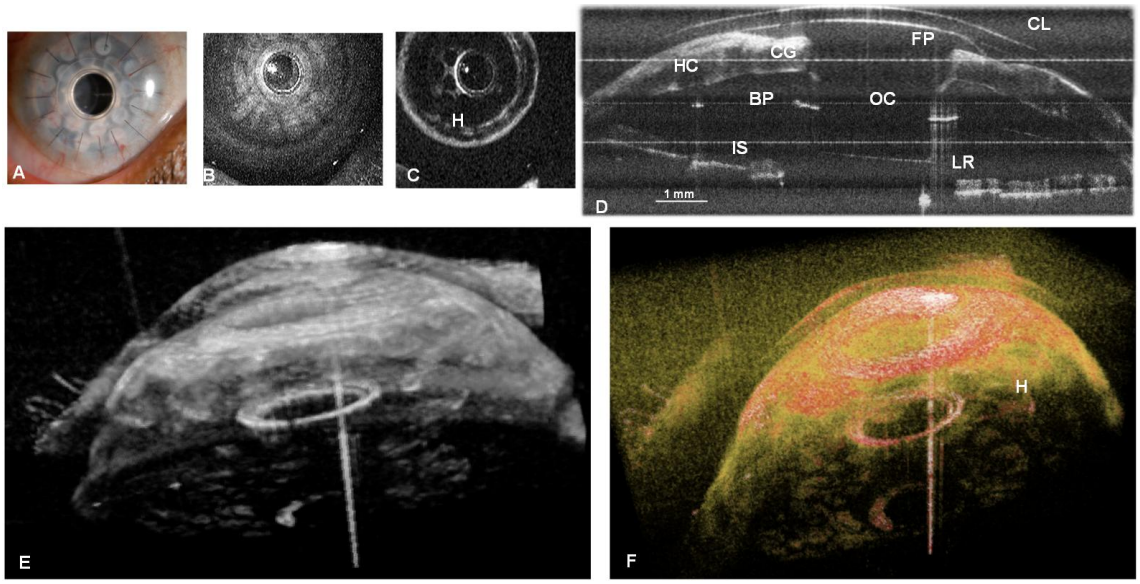

Fig. 6. Full imaging range mode: In-vivo implantation of type I KPro lens (A), en face view (3-D rendering) of implants (B), en face view of the back-plate of KPro (C); Cross-sectional images full KPro implants (D) lens [image comprise 2000 (lateral) x 2300 (axial) pixels spanning 14 mm (lateral) x 6.9 mm (axial), the latter scaled to account for refractive index. B-scan represents 2 averaged frames, FP: Front Plate, OC: Optical Cylinder, CG: Corneal Graft, BP: Back Plate, HC: Peripheral Host Cornea, LR: Lock Ring IS: Iris.]; Large-scale three-dimensional reconstruction of the anterior segment of human eye [E and F] in vivo: en face view (3-D rendering) [Images are reconstructed from 1000 × 100 × 2300 voxel data set. The size of the imaged volume is 15 × 20 × 7.5 mm.]

This information is improtant for studying the adaptation and orientation in anterior segment. We were able to distinguish precise components of the KPro and carrier graft as well as to visualize exquisitely the relationship of the epithelium to both the anterior and posterior surfaces of the KPro front plate. Holes on the back plate are clearly visible (Fig 6C). This imaging mode can be used to evaluate the components of the assembled KPro in vivo, with visualization of the donor cornea interface and to assess the presence of a potential space between the KPro front plate, the optical cylinder, and the corneal graft. Furthermore, we can explore in greater detail from the 3D reconstructed image, complications such as retroprosthetic membrane formation, epithelial downgrowth, stromal necrosis, and corneal thinning in 3D space.

4. Conclusion

In this paper we demonstrate a high-speed complex conjugate resolved 1 μm swept source optical coherence tomography system using coherence revival applied to ophthalmic imaging of the human anterior segment. This high-speed imaging, enable three-dimensional visualization of the anterior segment with a reduction motion artifact. This adjustable axial imaging range is important in the case of full anterior segment imaging. We were also able to demonstrate novel and highly detailed visual information for patients with a KPro compared with existing commercial imaging systems. The preliminary images obtained with this system demonstrate the possibility of high speed and high resolution imaging of large volumes associated with the KPro implants.

5. Acknowledgments

We gratefully acknowledge the contributions of VSRI UC Davis lab members. The help of Al-Hafeez Dhalla and Joseph A. Izatt, Department of Biomedical Engineering, Duke University, Durham, NC 27708, USA is greatly appreciated. This research was supported by the National Eye Institute (EY 014743) and Research to Prevent Blindness (RPB).

REFERENCES

[1] Maldonado, M. J., Ruiz-Oblitas, L., Munuera, J. M., Aliseda, D., García-Layana, A., and Moreno-Montañés, J., "Optical coherence tomography evaluation of the corneal cap and stromal bed features after laser in situ keratomileusis for high myopia and astigmatism," Ophthalmology 107(1), 81–87, discussion 88 (2000).

[2] Hoerauf, H., Wirbelauer, C., Scholz, C., Engelhardt, R., Koch, P., Laqua, H., and Birngruber, R., "Slit-lamp-adapted optical coherence tomography of the anterior segment," Graefes Arch. Clin. Exp. Ophthalmol. 238(1), 8–18 (2000).

[3] Wojtkowski, M., Leitgeb, R., Kowalczyk, A., Bajraszewski, T., and Fercher, A., "In vivo human retinal imaging by Fourier domain optical coherence tomography," J. Biomed. Opt. 7(3), 457–463 (2002).

[4] Fercher, A., Hitzenberger, C. K., Kamp, G., and El-Zaiat, S. Y., "Measurement of intraocular distances by backscattering spectral interferometry," Opt. Commun. 117(1-2), 43–48 (1995).

[5] Häusler, G., and Lindner, M. W., "'Coherence Radar' and 'Spectral Radar'—new tools for dermatological diagnosis," J. Biomed. Opt. 3(1), 21–31 (1998).

[6] Yun, S. H., Tearney, G., de Boer, J., and Bouma, B., "Motion artifacts in optical coherence tomography with frequency-domain ranging," Opt. Express 12(13), 2977–2998 (2004).

[7] Bajraszewski, T., Wojtkowski, M., Szkulmowski, M., Szkulmowska, A., Huber, R., and Kowalczyk, A., "Improved spectral optical coherence tomography using optical frequency comb," Opt. Express 16(6), 4163–4176 (2008).

[8] Wojtkowski, M., "High-speed optical coherence tomography: basics and applications," Appl. Opt. 49(16), D30–D61 (2010).

[9] Choma, M., Sarunic, M., Yang, C., and Izatt, J., "Sensitivity advantage of swept source and Fourier domain optical coherence tomography," Opt. Express 11(18), 2183–2189 (2003).

[10] http://www.heidelbergengineering.com/us/products/spectralis-models/resources/specifications/

[11] http://www.tomey.com/Products/OCT/SS-1000CASIA.html

[12] Yun, S., Tearney, G., de Boer, J., Iftimia, N., and Bouma, B., "High-speed optical frequency-domain imaging," Opt. Express 11(22), 2953–2963 (2003).

[13] Oh, W. Y., Yun, S. H., Tearney, G. J., and Bouma, B. E., "115 kHz tuning repetition rate ultrahigh-speed wavelength-swept semiconductor laser," Opt. Lett. 30(23), 3159–3161 (2005).

[14] Leung, M. K., Mariampillai, A., Standish, B. A., Lee, K. C., Munce, N. R., Vitkin, I. A., and Yang, V. X. D., "High-power wavelength-swept laser in Littman telescope-less polygon filter and dual-amplifier configuration for multichannel optical coherence tomography," Opt. Lett. 34(18), 2814–2816 (2009).

[15] Choma, M. A., Hsu, K., and Izatt, J. A., "Swept source optical coherence tomography using an all-fiber 1300-nm ring laser source," J. Biomed. Opt. 10(4), 044009 (2005).
[16] Huber, R., Wojtkowski, M., Taira, K., Fujimoto, J., and Hsu, K., "Amplified, frequency swept lasers for frequency domain reflectometry and OCT imaging: design and scaling principles," Opt. Express 13(9), 3513–3528 (2005).
[17] Huber, R., Wojtkowski, M., and Fujimoto, J., "Fourier Domain Mode Locking (FDML): A new laser operating regime and applications for optical coherence tomography," Opt. Express 14(8), 3225–3237 (2006).
[18] Eigenwillig, C. M., Wieser, W., Biedermann, B. R., and Huber, R., "Subharmonic Fourier domain mode locking," Opt. Lett. 34(6), 725–727 (2009).
[19] Huber, R., Adler, D. C., and Fujimoto, J., "Buffered Fourier domain mode locking: Unidirectional swept laser sources for optical coherence tomography imaging at 370,000 lines/s," Opt. Lett. 31(20), 2975–2977 (2006).
[20] Gora, M., Karnowski, K., Szkulmowski, M., Kaluzny, B. J., Huber, R., Kowalczyk, A., and Wojtkowski, M., "Ultra high-speed swept source OCT imaging of the anterior segment of human eye at 200 kHz with adjustable imaging range," Opt. Express 17(17), 14880–14894 (2009).
[21] Sarunic, M. V., Asrani, S., and Izatt, J. A., "Imaging the ocular anterior segment with real-time, full-range Fourier-domain optical coherence tomography," Arch. Ophthalmol. 126(4), 537–542 (2008).
[22] Wieser, W., Biedermann, B. R., Klein, T., Eigenwillig, C. M., and Huber, R., " Multi-Megahertz OCT: High quality 3D imaging at 20 million A-scans and 4.5 GVoxels per second," Optics Express, 18(14), 14685-14704 (2010).
[23] Adler, D. C., Huber, R., and Fujimoto, J. G., " Phase-sensitive optical coherence tomography at up to 370,000 lines per second using buffered Fourier domain mode-locked lasers," Optics Letters, 32(6), 626-628 (2007).
[24] Klein, T., Wieser, W., André, R., Pfeiffer, T., Eigenwillig, C. M., Huber R., "Multi-MHz FDML OCT: snapshot retinal imaging at 6.7 million axial-scans per second," Proc. SPIE 8213, Optical Coherence Tomography and Coherence Domain Optical Methods in Biomedicine XVI, 82131E (2012).
[25] Yasuno, Y., Madjarova, V. D., Makita, S., Akiba, M., Morosawa, A., Chong, C., Sakai, T., Chan, K. P., Itoh, M., and Yatagai, T., "Three-dimensional and high-speed swept-source optical coherence tomography for in vivo investigation of human anterior eye segments," Opt. Express 13(26), 10652–10664 (2005).
[26] Karnowski, K., Kaluzny, B. J., Szkulmowski, M., Gora, M., and Wojtkowski, M., "Corneal topography with high-speed swept source OCT in clinical examination," Biomedical Optics Express 2(9), 2709-2720 (2011).
[27] Dohlman, C.H., Doane, M.G., "Some factors influencing outcome after keratoprosthesis surgery," Cornea, 13, 214-218 (1994).
[28] Doane, M. G., Dohlman, C. H., "Fabrication of a keratoprosthesis," Cornea, 15, 179-184 (1996).
[29] Julian, P. S., Garcia et al, "Evaluation of the Stability of Boston Type I Keratoprosthesis-Donor Cornea Interface Using Anterior Segment Optical Coherence Tomography," Clinical Science 29 (9), 1031-1035 (2010).
[30] Alzaga, A. G., Radcliffe, N. M., Sippel, K. C., "Boston type I keratoprosthesis-donor cornea interface evaluated by high-definition spectral-domain anterior segment optical coherence tomography," Clinical Ophthalmology, 6, 1355-1359, (2012).
[31] Klein, T., Wieser, W., Eigenwillig, C. M., Biedermann, B. R., and Huber, R., "Megahertz OCT for ultrawide-field retinal imaging with a 1050nm Fourier domain mode-locked laser," Optics Express, 19(4), 3044-3062 (2011).
[32] Dhalla, A. H., Nankivil, D., and Izatt, J. A., "Complex conjugate resolved heterodyne swept source optical coherence tomography using coherence revival," Biomed. Opt. Express 3, 633-649 (2012).